Princeton Plasma Physics Laboratory

PPPL-

PPPL-

**PRINCETON
PLASMA PHYSICS
LABORATORY**

Princeton Plasma Physics Laboratory
Report Disclaimers

Full Legal Disclaimer

This report was prepared as an account of work sponsored by an agency of the United States Government. Neither the United States Government nor any agency thereof, nor any of their employees, nor any of their contractors, subcontractors or their employees, makes any warranty, express or implied, or assumes any legal liability or responsibility for the accuracy, completeness, or any third party's use or the results of such use of any information, apparatus, product, or process disclosed, or represents that its use would not infringe privately owned rights. Reference herein to any specific commercial product, process, or service by trade name, trademark, manufacturer, or otherwise, does not necessarily constitute or imply its endorsement, recommendation, or favoring by the United States Government or any agency thereof or its contractors or subcontractors. The views and opinions of authors expressed herein do not necessarily state or reflect those of the United States Government or any agency thereof.

Trademark Disclaimer

Reference herein to any specific commercial product, process, or service by trade name, trademark, manufacturer, or otherwise, does not necessarily constitute or imply its endorsement, recommendation, or favoring by the United States Government or any agency thereof or its contractors or subcontractors.

PPPL Report Availability

Princeton Plasma Physics Laboratory:

http://www.pppl.gov/techreports.cfm

Office of Scientific and Technical Information (OSTI):

http://www.osti.gov/bridge

Related Links:

U.S. Department of Energy

Office of Scientific and Technical Information

Fusion Links

Transverse focusing of intense charged particle beams with chromatic effects for heavy ion fusion[☆]

James M. Mitrani*, Igor D. Kaganovich, Ronald C. Davidson

Princeton Plasma Physics Laboratory, Princeton University, Princeton, NJ, 08543, USA

Abstract

A final focusing scheme designed to minimize chromatic effects is discussed. The Neutralized Drift Compression Experiment-II (NDCX-II) will apply a velocity tilt for longitudinal bunch compression, and a final focusing solenoid (FFS) for transverse bunch compression. In the beam frame, neutralized drift compression causes a sufficiently large spread in axial momentum, p_z, resulting in chromatic effects to the final focal spot during transverse bunch compression. Placing a weaker solenoid upstream of a stronger final focusing solenoid (FFS) mitigates chromatic effects and improves transverse focusing by a factor of approximately 2-4 for appropriate NDCX-II parameters.

Keywords: Solenoid focusing, Bunched beam, Chromatic effects

1. Introduction

One of the challenges for the Neutralized Drift Compression Experiment II (NDCX-II) and heavy ion fusion (HIF) is longitudinally and transversely compressing an intense ion charge bunch, in order to maximize fluence and current density on the target [1, 2]. Neutralized drift compression [3, 4] longitudinally compresses the beam with an induction module applying a variable voltage waveform, which decelerates the particles at the head of the charge bunch, and accelerates the particles at the tail of the charge bunch, resulting in significant longitudinal compression. Due to conservation of emittance, the longitudinally compressed charge bunch contains a larger spread in p_z-space (Fig. 1). Unfortunately, the large spread in axial momentum, p_z, complicates transverse focusing, as particles with different values of p_z are focused at different axial locations. Therefore, given a large spread in p_z, final focusing schemes for NDCX-II should mitigate chromatic effects caused by the velocity tilt to improve transverse focusing. This paper is organized as follows: Section 2 describes analytical calculations for solenoid focusing using the thin lens approximation; Section 3 shows the results of a two solenoid focusing scheme using appropriate NDCX-II parameters; and Section 4 discusses the above results.

2. Theoretical Model

2.1. Thin lens calculations of solenoid focusing

A brief derivation of solenoid focusing for non-relativistic beams using the thin lens approximation is presented here,
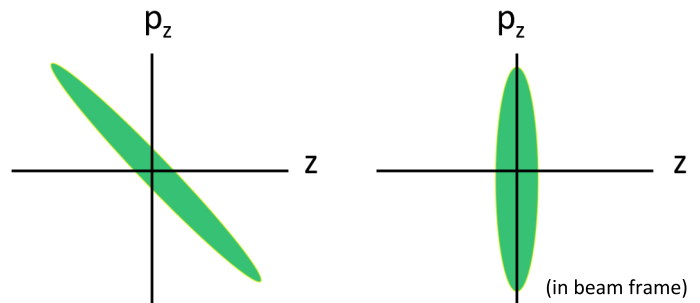

Figure 1: Beam distribution in (z,p_z) space. The velocity tilt [3] longitudinally compresses the beam bunches in z space. The compressed beam bunches have a larger spread in p_z-space.

in order to anlayze chromatic effects on the final focal radius, R_{sp}, and to assist in the design of a final focusing system for appropriate NDCX-II parameters. The thin lens approximation allows for compact analytical calculations of emittance and chromatic effects on the final focusing radius, and assumes $\kappa l \ll 1$, where l is the solenoid length, and $\kappa(z) = qB(z)/2p_z = qB(z)/\sqrt{8MqU}$ is the solenoid force focusing function, and $B(z)$, q, and M are the solenoid's axial magnetic field, ion charge, and ion mass respectively, and $qU = p_z^2/2M$ is the ion kinetic energy. Since $\kappa l \sim 0.6$ for the final focusing solenoids used for NDCX-II (Table 1), calculations using the thin lens approximation aren't perfectly accurate. Nevertheless, these calculations do provide a clear picture of the physics behind emittance and chromatic effects on R_{sp}.

Solenoid focusing of charged particle beams is well understood [5, 6], and is axisymmetric. For non-relativistic axisymmetric, uniform beams with no self field, $K_b=0$, the

equations of transverse motion are,

$$x''(z) - 2\Omega_L(z)y'(z) - \Omega'_L(z)y(z) = 0, \quad (1a)$$
$$y''(z) + 2\Omega_L(z)x'(z) + \Omega'_L(z)x(z) = 0, \quad (1b)$$

where, $x(z)$ and $y(z)$ are the particles' transverse position, $\Omega_L(z)$=qB(z)/2p_z is the normalized Larmor frequency (relativistically, Ω_L=qB/2Mc$\gamma\beta$), and primes indicate derivatives with respect to z. One can simplify Eq. (1) by using the following transformation,

$$X(z) = x(z)\cos\theta_L(z) + y(z)\sin\theta_L(z), \quad (2a)$$
$$Y(z) = -x(z)\sin\theta_L(z) + y(z)\cos\theta_L(z), \quad (2b)$$

where $\theta_L(z) = -\int_{z_0}^{z} dz'\Omega_L(z')$, to transform to the Larmor frame, and obtain the paraxial ray tracing equation,

$$X''(z) = -\kappa^2(z)X(z), \quad (3a)$$
$$Y''(z) = -\kappa^2(z)Y(z), \quad (3b)$$

where $[\kappa(z)]^2 = [\Omega_L(z)]^2$, and is defined previously. For solenoids, $B(z)$ is constant inside the solenoid, and sharply decays to 0 outside the solenoid. The following derivations use the "hard-edge" approximation, where $\kappa(z) = \kappa_0 = qB_0/2p_z$ inside the solenoid and zero outside. Using Eq. (3), particles entering a solenoid with an initial radius r_0 and no initial angle, $r'_0 = 0$, are focused with an angle $r' = -r_0\kappa\sin(\kappa l)$, resulting in a focal length of,

$$F_z = -\frac{r_0}{r'} \approx (\kappa^2 l)^{-1}. \quad (4)$$

The emittance-limited final focal radius for beams with finite emittance is,

$$R_{sp} \approx \frac{\epsilon F_z}{R_0}, \quad (5)$$

which can be derived from the space-charge-free envelope equation [See Eq. (10)]. Beams with chromatic effects have particles with different focal lengths, as shown in Figure 4, which increases the final focal spot, R_{sp}. For a single solenoid, chromatic effects on R_{sp} have the form,

$$R_{sp} \approx \beta\delta F_z \approx R_0\frac{\delta E}{E}, \quad (6)$$

where β (assumed small) is the angle of approach for a particle at the edge of the beam, δF_z is the difference in focal lengths for particles with different values of p_z, R_0 is the initial beam radius (no initial angle is assumed), and $\delta E/E$ is the kinetic energy spread in the beam ($\delta E/E \approx 2\delta p_z/p_z$). Since the ratio of chromatic effects to emittance effects, $(R_0\delta E/E)/(\epsilon F/R_0)$, is >100 for typical NDCX-II parameters (Table 1), a final focusing system for NDCX-II should mitigate chromatic effects to improve transverse focusing.

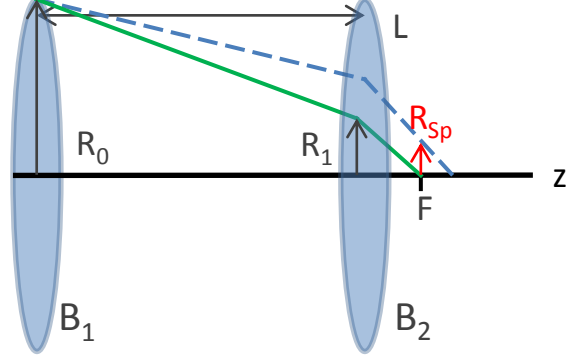## 2.2. Thin Lens Calculations: Optimum Distance Between Two Solenoids

Figure 2: Chromatic effects on final focusing spot R_{sp}, in a two-solenoid final focusing scheme. Two solenoids, with magnetic field strengths B_1 and B_2 are separated by a distance L. The solid (green) lines represent a trajectory for a particle with energy E_0 (or momentum p_{z0}). The solenoid focal lengths for a particle with energy E_0 are F_1 and F_2 [$F \approx (\kappa^2 l)^{-1}$, and κ=qB/2p_z]. The effective focal length for both solenoids is F, and is shown in the Figure. The dashed (blue) line represents a particle with kinetic energy $E_0+\delta E$ (or momentum $p_{z0}+\delta p_z$). The solenoid focal lengths for a particle with energy $E_0 + \delta E$ are F_{1s} and F_{2s}, where $F_{\alpha s} \approx F_\alpha(1 + \delta E/E)$, $\alpha = 1, 2$. The resulting focal radius, R_{sp} is defined in Eq. (6).

Figure 2 shows particle trajectories in the presence of two solenoids separated by a distance L. The solid (green) line represents a normal trajectory for a particle on the edge of the beam with energy E_0, and the dashed (blue) line represents a shifted trajectory for a particle with energy $E_0+\delta E$. The magnetic field strengths are B_1 and B_2, such that $B_2>B_1$. (Note that in Figure 2, that L is slightly less than the focal length of the first solenoid, F_1, resulting in an underfocused beam entering the second solenoid.

Using the thin lens approximation, in the presence of two solenoids, the final focal radius is,

$$R_{sp} = r_1 + r'_{1+}(F - L); \quad (7a)$$
$$r_1 = R_0 + r'_{0+}L, \quad (7b)$$
$$F - L = \frac{F_2(F_1 - L)}{F_2 + F_1 - L}, \quad (7c)$$
$$r'_{1+} = -\frac{R_0}{F_{1s}} + -\frac{r_1}{F_{2s}}, \quad (7d)$$

where r_1 is the radius of the *shifted* particle as it enters the second solenoid, F is the effective focal length of the two solenoids, r'_{1+} is the angle of the *shifted* particle as it leaves the 2nd solenoid, and F_{1s} and F_{2s} are the individual focal lengths for the shifted particles, $F_{1s} = F_1(1 + \delta E/E)$. By taking the derivative of Eq. (7a) with respect to L, one can show that the optimum distance for transverse focusing for given values of F_1 and F_2, is given by,

$$L_{opt} = F_1 + F_2 - \sqrt{F_1 F_2 + F_2^2}. \quad (8)$$

Typical NDCX-II Parameters			
ϵ	2.25 mm-mrad	KE	3 MeV
M (Li$^+$ Ions)	$7 \cdot M_P$	q	+1 C
R_0	30 mm	R_0'	0
B (FFS)	8 T	l (FFS)	10 cm
κ (FFS)	6.04 m^{-1}	$\delta E/E$	20%

Table 1: Parameters used for this study. The values of B, l, and κ are realistic strength parameters for an NDCX-II final focusing solenoid (FFS) [2]. In the table, $\delta E/E$ is the spread in beam energy due to the applied velocity tilt. The corresponding spread in $\delta p_z/p_z$ is $\approx \pm 10\%$.

3. Results of the analysis

3.1. Typical parameters for NDCX-II beams

Table 1 shows typical parameters relevant to NDCX-II. A 3 MeV Li$^+$ ion beam, with an emittance of 2.25 mm-mrad was assumed. The beam is assumed to enter the final focusing solenoid(s) with an initial radius of 30mm, and no initial angle. The NDCX-II solenoids will be 10cm in length, and use copper coils with copper shielding designed to limit magnetic fringe field effects; the form of the assumed magnetic field, B(z), is plotted in Fig. 4 [1]. Magnetic field strengths of 8T and 16T are considered for the final focusing solenoid. Neutralized drift compression is assumed [3], and self field effects are ignored in these calculations.

3.2. Effective beam radius

Varying criteria are used to determine the effectiveness of a final focusing system. The above analytic derivations assumed a beam with a fixed initial radius, R_0, and calculated the final focal radius, R_{sp}, which was assumed to contain 100% of the beam particles. However, a goal for NDCX-II is to maximize particle fluence within set radii. Therefore, depending on the beam's initial density distribution, the effectiveness of a final focusing system might be better determined by minimizing parameters such as R_{50} or R_{90}, the radius containing 50% or 90% of the beam particles. The full width at half maximum, $fwhm$, is a traditional method for comparing beam distributions, and is included in this study. In addition to the $fwhm$, the percentage of beam particles within the $fwhm$ is also calculated. (That is, a density distribution with a narrow $fwhm$ but a low percentage of beam particles within the $fhwm$ would most likely have a lower energy density at the target.)

The quantity R_{100} was numerically calculated using the space-charge-free envelope equations. The space-charge-free envelope equations can be obtained from Courant-Snyder theory, by substituting the generic solution,

$$X_i(z) = A_i w(z)\cos(\psi(z) + \phi_i), \qquad (9a)$$
$$Y_i(z) = A_i w(z)\sin(\psi(z) + \phi_i), \qquad (9b)$$

into Eq. (3). The envelope equation is therefore [5],

$$r''(z) = -\kappa(z)^2 r(z) + \frac{\epsilon^2}{r(z)^3}, \qquad (10)$$

and can be used to define an effective beam radius. Because $\kappa(z)$ is a function of beam energy, the envelope equation can only represent one beam slice in energy space. To account for chromatic effects, Fig. 4 shows plots of three beam envelopes, with energies E_0 and $E_0 \pm \delta E$. The dotted black curves in Fig. 4 represents the maximum absolute value of the envelopes, and all beam particle trajectories are "enveloped" by these curves. Therefore, the beam radius containing 100% of beam particles, R_{100}, is calculated by numerically solving the envelope equations.

All other results in Table 3 were calculated by numerically solving many (10^4) individual particle trajectories [Eq. (3)]. Using a Monte-Carlo like method, individual particle trajectories, each with a random amplitude A_i and phase ϕ_i fixed within the conservation of emittance, were numerically calculated to solve for a density distribution, $n_F(x)$, at the focal point. From $n_F(x)$, results such as the value of $fwhm$, the percentage of beam particles within $fwhm$, and the values of R_{50} and R_{90}, were easily determined.

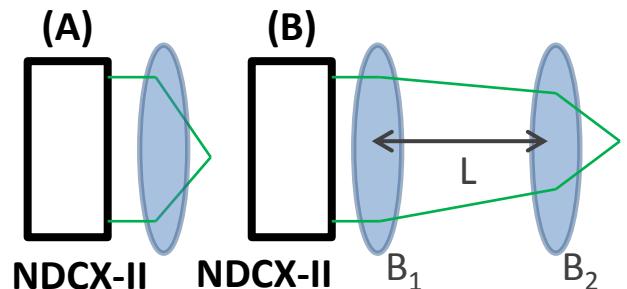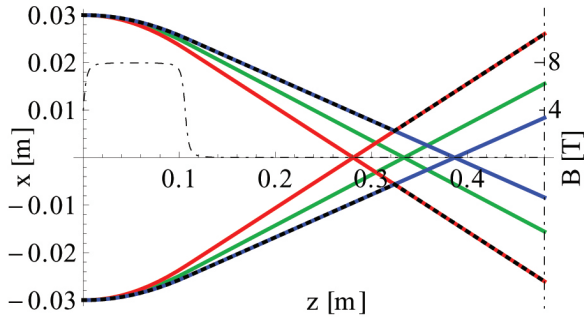### 3.3. Beam focusing using two solenoids

Figure 3: Layout of transverse focusing schemes being considered. Both final focusing schemes assume the beam has been created, accelerated, passed through the velocity tilt inductor, and undergone neutralized drift compression. The left scheme (A) uses a single focusing solenoid for transverse focusing. The right scheme (B) uses two solenoids, with B$_1$ < B$_2$, separated by distance L, to mitigate chromatic effects. The solid (green) lines trace out the beam envelopes.

Figure 3 shows two possible transverse focusing schemes. A simple transverse focusing scheme would consist of one strong final focusing solenoid (FFS). Given the beam parameters in Table 1, in the absence of chromatic effects ($\delta E/E=0$), a single 8T FFS will focus the beam to a focal radius of ~22 microns. However, if the velocity tilt in the induction module produces a $\pm 20\%$ spread in beam energy, the final focal radius increases to 5.6mm! Figures 4(a) and 6 (dashed lines) both show that increasing the magnetic field strength of the FFS has a negligible effect on the final focus radius. Figure 4(a) shows the envelopes

(a) One final focusing solenoid scheme, where B=8T.
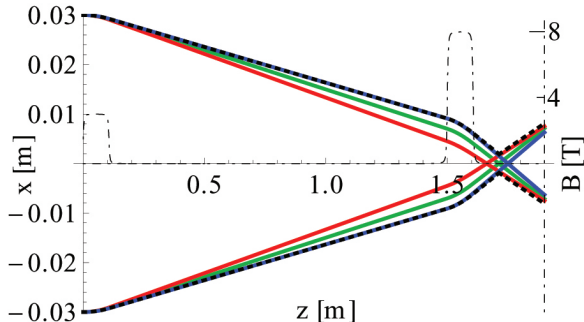
(b) Two solenoid scheme, where B_1=3T, and B_2=8T. The solenoids are separated by a distance of L=1.5m.

Figure 4: The green, blue, and red envelopes represent three beam slices, where the beam energy is E_0, $E_0 + \delta E$, and $E_0 - \delta E$, E_0=3MeV, and $\delta E/E$=0.2. The dashed gray curves represent the form of $B(z)$ used for the solenoids' magnetic field. The effective lengths of the solenoids, $l = B_0^{-2} \int dz B^2(z)$ [6], are 10cm.

[Eq. (10)] for three beam slices. As stated previously, the green envelope represents the beam slice with energy $E_0 = 3$ MeV, and would define the beam radius in the absence of chromatic effects. The blue and red envelopes represent beam slices with energies of $E_0 \pm \delta E$, where $\delta E/E$=20% (analogous to blue and red shifted particles). The dotted black envelope defines the effective beam radius with chromatic effects, which are clearly visible on the final focal radius, R_{sp}.

Figure 6 shows plots versus r of the normalized integrated radial beam density, defined as

$$I(r) = \frac{\int_0^r dr' r' n(r')}{\int_0^{+\infty} dr' r' n(r')}. \tag{11}$$

Figure 6 (dashed lines) and Table 3 show that increasing the FFS magnetic field strength provides only slightly better focusing.

Figures 4(b) and 6 (solid lines) show that the two-solenoid scheme significantly improves transverse focusing. The optimum distance, L, between the two solenoids was analytically calculated using the thin lens approximation [Eq. (8)], and numerically calculated using finite lens lengths (Figure 5). The results are compared in Table 2.

Two-Solenoid Final Focusing Scheme		
Optimum Distance, L		
B_2	8 T	16 T
Eq. (8)	1.45 m	1.63 m
Fig. 5	1.5 m	1.7 m

Table 2: Optimum distance, L, between the solenoids, for the two-solenoid final focusing scheme (Fig. 3). The value of B_1 is fixed at 3T, and all parameters are in Table 1. Note that Eq. (8) relies on the thin-lens approximation, whereas Figure 5 uses finite lens lengths.
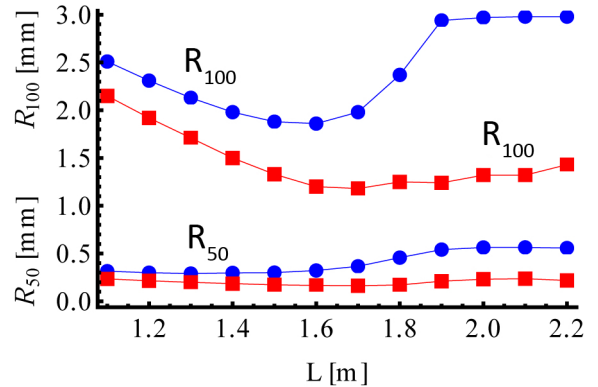

Figure 5: Values of R_{50} and R_{100} with varying values for the distance, L, between two solenoids, in a two solenoid final focusing scheme. B_1 is fixed at 3T, for all data points shown in the Figure. The value of B_2 is 8T for the circle (blue) points, and B_2=16 T for the square (red) points. From the above graph, the optimum values for L are L=1.5m for B_2=8T, and L=1.7m for B_2=16T. [Eq. (8) gives values of L=1.45m for B_2=8T, and L=1.63m for B_2=16T.] All other values are the same as in Table 1.

In the two-solenoid scheme, given typical NDCX-II parameters, the focal length of the first B_1=3T solenoid is ~2m. Therefore, the beam is underfocused before entering the second solenoid.

Figure 6 compares the normalized integrated radial density [Eq. (11)] for the one- and two-solenoid schemes, showing a significant improvement in transverse focusing for the two solenoid scheme for B_2=8T, and B_2=16T. Table 3 shows that the two-solenoid scheme improves transverse focusing by a factor of ~2 for R_{50}, and a factor of ~3 for R_{100} for 8T final focusing solenoids. The results for 16T final focusing solenoids are even better, as the two-solenoid scheme improves transverse focusing by a factor of ~3 for R_{50}, and a factor of ~4 for R_{100}.

4. Discussion

A two-solenoid final focusing scheme mitigates chromatic effects, resulting in a smaller final focal radius, R_{sp}. Equation (5) shows that in the absence of chromatic effects, the final focal radius R_{sp} is inversely proportional to R_0. However, in the presence of strong chromatic effects, where $R_0 \delta E/E \gg \epsilon F_z/R_0$, the value of R_{sp} is roughly proportional to R_0, and decreasing the initial beam radius before the beam enters the final focusing solenoid leads to a smaller focal spot.

4

Results	One Solenoid			Two Solenoids	
B-field [T]	3T	8T	16T	8T	16T
$fwhm$ [mm]	0.30	0.22	0.20	0.30	0.20
$fwhm$ [%]	*23*	*20*	*20*	*34*	*38*
R_{50} [mm]	0.55	0.54	0.46	0.30	0.16
R_{90} [mm]	1.7	1.7	1.5	0.88	0.48
R_{100} [mm]	6.0	5.6	4.9	1.9	1.2

Table 3: For the two-solenoid focusing scheme, magnetic field strengths of B_1=3T and B_2=8T, and B_1=3T and B_2=16T are considered. The value of $fwhm$ is a rough estimate, of the full width at half maximum, for the density distribution, $n_F(x)$, at the focal spot. The percentage of beam particles within the $fwhm$ is also included. The values of R_{50}, R_{90}, and R_{100}, are the radii containing 50%, 90%, and 100% of the beam particles, respectively. [R_{100} is an effective beam radius, and was calculated from the envelope equation, Eq. (10).] These results are from the one-solenoid and two-solenoid final focusing schemes (Fig. 3), with different magnetic field strengths. The distance L between the two solenoids was L=1.5m for B_2=8T, and L=1.7m for B_2=16T.
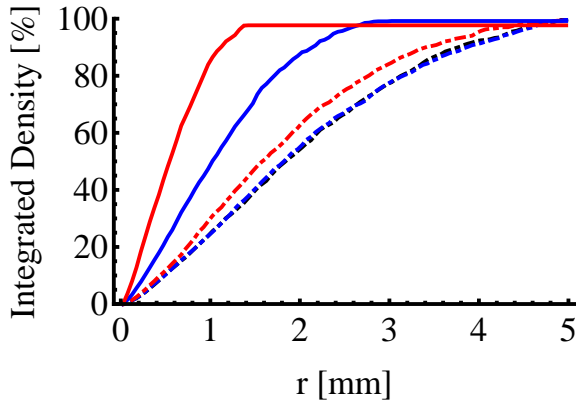

Figure 6: Normalized integrated radial density plots [Eq. (11)] for a one-solenoid final focusing scheme (dotted lines), and for a two-solenoid final focusing scheme (solid lines). The black, blue, and red colors represent final focusing solenoid magnetic field strengths of 3T, 8T, and 16T, respectively.

Effects such as radial misalignments, emittance growth [7], coupling between transverse and longitudinal emittance [8], or other effects that limit longitudinal compression [9, 10] were not considered in this study. Any effects that limit longitudinal compression would result in a smaller spread in p_z-space (Figure 1), and reduced chromatic effects on R_{sp}.

We have proposed using a two solenoid focusing scheme for beams with typical NDCX-II parameters. Neutralized drift compression was assumed, resulting in a narrow beam distribution in z-space, and a large spread in p_z-space. For beams with a sufficiently large spread in p_z, the two-solenoid focusing scheme improves transverse focusing by a factor of approximately 2-4 relative to a one-solenoid final focusing scheme.

References

[1] A. Friedman, J. Barnard, R. Cohen, D. Grote, S. Lund, W. Sharp, A. Faltens, E. Henestroza, J. Jung, J. Kwan, E. Lee, M. Leitner, B. Logan, J. Vay, W. Waldron, R. Davidson, M. Dorf, I. Kaganovich, Phys. Plasmas 17 (2010) 056704.

[2] P. Seidl, A. Anders, F. Bieniosek, J. Barnard, J. Calanog, A. Chen, R. Cohen, J. Coleman, M. Dorf, E. Gilson, et al., Nucl. Instr. and Meth. in Phys. Res. Sect. A 606 (2009) 75–82.

[3] P. Roy, S. Yu, E. Henestroza, A. Anders, F. Bieniosek, J. Coleman, S. Eylon, W. Greenway, M. Leitner, B. Logan, et al., Phys. Rev. Lett. 95 (2005) 234801.

[4] D. Welch, D. Rose, T. Genoni, S. Yu, J. Barnard, Nucl. Instr. and Meth. in Phys. Res. Sect. A 544 (2005) 236–242.

[5] R. Davidson, H. Qin, Physics Of Intense Charged Particle Beams In High Energy Accelerators, World Scientific, Singapore, 2001.

[6] M. Reiser, P. O'Shea, S. Bernal, R. Kishek, Theory and design of charged particle beams, Wiley, New York, 1994.

[7] E. Gilson, R. Davidson, M. Dorf, P. Efthimion, R. Majeski, M. Chung, M. Gutierrez, A. Kabcenell, Physics of Plasmas 17 (2010) 056707.

[8] H. Qin, R. Davidson, M. Chung, J. Barnard, T. Wang, in: Proc. of the 2011 Particle Accelerator Conference, New York, NY, p. 758.

[9] I. Kaganovich, S. Massidda, E. Startsev, R. Davidson, J. Vay, A. Friedman, Nucl. Instr. and Meth. in Phys. Res. Sect. A 678 (2012) 48.

[10] A. Sefkow, R. Davidson, Phys. Rev. Spec. Top.-Acceler. Beams 10 (2007) 100101.